Atmos. Meas. Tech. Discuss., 7, 12517–12543, 2014
www.atmos-meas-tech-discuss.net/7/12517/2014/
doi:10.5194/amtd-7-12517-2014

Atmospheric Measurement Techniques Discussions

Comparison of GOME-2/Metop total column water vapour with ground-based and in situ measurements

N. Kalakoski[1], J. Kujanpää[1], V. Sofieva[1], J. Tamminen[1], M. Grossi[2], and P. Valks[2]

[1]Finnish Meteorological Institute, Helsinki, Finland
[2]Institut für Methodik der Fernerkundung (IMF), Deutsches Zentrum für Luft- und Raumfahrt (DLR), Oberpfaffenhofen, Germany

Received: 5 September 2014 – Accepted: 21 October 2014 – Published: 12 December 2014

Correspondence to: N. Kalakoski (niilo.kalakoski@fmi.fi)

Published by Copernicus Publications on behalf of the European Geosciences Union.

Abstract

Total column water vapour product from the Global Ozone Monitoring Experiment-2 on board Metop-A and Metop-B satellites (GOME-2/Metop-A and GOME-2/Metop-B) produced by the Satellite Application Facility on Ozone and Atmospheric Chemistry Monitoring (O3M SAF) is compared with co-located radiosonde and Global Positioning System (GPS) observations. The comparisons are performed using recently reprocessed data by the GOME Data Processor (GDP) version 4.7.

The comparisons are performed for the period of January 2007–July 2013 (GOME-2A) and from December 2012 to July 2013 (GOME-2B). Radiosonde data are from the Integrated Global Radiosonde Archive (IGRA) maintained by National Climatic Data Center (NCDC) and screened for soundings with incomplete tropospheric column. Ground-based GPS observations from COSMIC/SuomiNet network are used as the second independent data source.

Good general agreement between GOME-2 and the ground-based observations is found. The median relative difference of GOME-2 to radiosonde observations is −2.7 % for GOME-2A and −0.3 % for GOME-2B. Against GPS observations, the median relative differences are 4.9 and 3.2 % for GOME-2A and B, respectively. For water vapour total columns below 10 kg m^{-2}, large wet biases are observed, especially against GPS observations. Conversely, at values above 50 kg m^{-2}, GOME-2 generally underestimates both ground-based observations.

1 Introduction

Water vapour is the most important greenhouse gas: it accounts for about 60 % of the greenhouse effect (e.g., Kiehl and Trenberth, 1997). The knowledge of spatio-temporal distribution and variability of water vapour is very important for assessment of climate change. Since ground-based observations do not provide uniform global coverage (in particular, they are scarce over oceans and in polar areas), satellite observations are

necessary to fill these gaps. Water vapour has been measured from space using several different instruments. Long time series over ocean are available from microwave radiometers such as Special Sensor Microwave/Imager (SSM/I) (e.g., Schlüssel et al., 1990) and its successor Special Sensor Microwave Imager/Sounder (SSMIS). In the near-infrared band, observations are available from radiometers such as Medium Resolution Imaging Spectrometer (MERIS) (e.g., Bennartz et al., 2001) and Moderate Resolution Imaging Spectroradiometer (MODIS) (e.g., King et al., 1992; Gao et al., 2003). Long-term water vapour observations in the infrared band are available from instruments such as TIROS Operational Vertical Sounder (TOVS), Advanced TOVS (ATOVS) and Atmospheric Infrared Sounder (AIRS) (e.g., Chaboureau et al., 1998; Li et al., 2000; Susskind et al., 2003). Global Positioning System (GPS) radio occultation data from Constellation Observing System for Meteorology, Ionosphere, and Climate (COSMIC) mission have also been used to derive atmospheric water vapour (e.g., Anthes et al., 2008).

Water vapour can be also measured using observations at UV and visible wavelengths. UV/VIS spectrometers Global Ozone Monitoring Experiment instrument aboard European Remote Sensing Satellite-2 (GOME/ERS-2) (Noël et al., 1999, 2002) and Scanning Imaging Absorption spectrometer for Atmospheric Chartography (SCIAMACHY) (Noël et al., 2004) provide observations from mid-1990s. Operating at visible wavelengths, these instruments can observe the atmospheric water vapour columns over all surfaces, and have the advantage of high sensitivity to water vapour layers close to the surface. This makes the UV/VIS observations useful in studies of tropospheric water vapour trends and variability.

Satellite observations are subject to their own limitations, depending on the measurement techniques. While UV/VIS sensors operate in daylight conditions and are usually limited by the presence of clouds, the microwave measurements are typically limited to ocean areas and infrared observations have the disadvantage of being less sensitive to surface emissions from lower atmospheric layers compared to UV/VIS observations.

Global Ozone Monitoring Experiment-2 (GOME-2) is a nadir-viewing scanning spectrometer aboard EUMETSATs Metop-A and B satellites (hereafter referenced as GOME-2A and GOME-2B, respectively) launched in October 2006 and September 2012, respectively, followed by the third instrument aboard Metop-C, due to be launched in 2017. Metop series forms the space segment of the EUMETSAT Polar System (EPS), expected to operate at least until 2020. GOME-2 is dedicated to observation of atmospheric trace gases, mainly total ozone column and vertical ozone profiles. Other retrieved parameters include total columns of nitrogen dioxide, sulphur dioxide, water vapour, bromine oxide and other trace gases, as well as aerosols. The Metop-A and B orbit is sun-synchronous with the equator crossing time of 9.30 a.m. local time. Processing, dissemination and archiving of GOME-2 data products is handled by the EUMETSAT Satellite Application Facility on Ozone and Atmospheric Chemistry Monitoring (O3M SAF). O3M SAF water vapour data is available from January 2007 onwards.

O3M SAF GOME-2A water vapour has previously been compared with data from SCIAMACHY on board Envisat (Noël et al., 2008), which uses a similar retrieval scheme. It was found that GOME-2A and SCIAMACHY data are in good agreement, with the correlation coefficient of 0.99 and the mean bias of 0.5 $\mathrm{kg\,m^{-2}}$. Recently, Grossi et al. (2014) provided detailed description of the improved GOME-2A and B algorithm and compared it to SSMIS measurements, combined SSM/I + MERIS dataset and ECMWF model data. Good general agreement was reported with all three datasets with mean bias of $\pm 0.35\,\mathrm{kg\,m^{-2}}$ against all independent datasets analysed, although some seasonal and regional biases have been identified.

The water vapour products from GOME/ERS-2 and SCIAMACHY instruments, which use similar measurement principles and retrieval algorithms as the one used for GOME-2, have been extensively validated against SSM/I observations. Data have been found to generally slightly underestimate the water vapour columns from the SSM/I observations. The underestimation is more significant in cloudy conditions, especially in winter. The SD of differences for observations is generally 3–5 $\mathrm{kg\,m^{-2}}$. In clear-sky con-

dition, a good agreement is found (Noël et al., 1999; Wagner et al., 2003; Noël et al., 2005; Wagner et al., 2005, 2006; Mieruch et al., 2010). Du Piesanie et al. (2013) validated SCIAMACHY water vapour retrievals against radiosonde data and discussed the effect of clouds in water vapour retrievals.

This paper is dedicated to the geophysical validation of the GOME-2 water vapour total column against radiosonde and ground-based GPS measurements. The paper is organized as follows. In Sect. 2, we give a brief description of the GOME-2 instrument and the water vapour retrieval. Section 3 describes data used in comparisons and Sect. 4 the data selection and co-location criteria. The validation results are presented and discussed in Sect. 5. The summary concludes the paper.

2 GOME-2 instrument and water vapour retrieval

GOME-2 sensors measure solar light scattered from the Earth's atmosphere and reflected from the surface at ultraviolet and visible wavelengths (240–790 nm) with a spectral resolution of 0.2–0.4 nm. GOME-2 has the spatial resolution of 40 km × 80 km with the swath width of 1920 km, which provides daily global coverage at mid-latitudes. Each 6 s scan cycle consists of the 4.5 s forward scan (twenty four 40 km × 80 km pixels) and the 1.5 s back-scan (eight 40 km × 240 km pixels). The data from both forward and back-scan pixels are processed and written into data files (at the moment, the data from back-scans are not recommended for use). At low solar elevation angles, longer integration times are used, which results in an increased pixel size. Additionally, for one day (the 15th day) in every 29 day observation cycle, the GOME-2A measures at narrow swath (320 km) mode. Since 15 July 2013, GOME-2A is operating in tandem mode with GOME-2B, with GOME-2A measuring with 960 km swath width and 40 km*x*40 km pixel size and GOME-2B measuring with 1920 km swath width and 40 km × 80 km pixel size.

The GOME-2 water vapour total column data are aimed mainly for climatological studies. In contrast to near-infrared and GPS radio-occultation measurements, the retrieval algorithm uses no external input on the state of the atmosphere. Thus GOME-2 data are fully independent of measurements from other instruments and/or modelling at a cost of possible larger uncertainties of individual measurements.

The retrieval uses the Differential Optical Absorption Spectroscopy (DOAS) algorithm with the 614–683 nm fitting window to get slant columns of atmospheric water vapour, followed by a non-linearity absorption correction and finally by the Air Mass Factor (AMF) conversion to generate vertical total columns. The air mass correction factor is determined using O_2 absorption in the same fitting window. The detailed description of the algorithm and data can be found in Algorithm Theoretical Basis Document and Product User Manual available at the O3M SAF website (Valks et al., 2013a, b), as well as in the recent paper by Grossi et al. (2014).

3 Ground-based data sources

Integrated Global Radiosonde Archive (IGRA) is a radiosonde dataset maintained by National Climatic Data Center (NCDC) (http://www.ncdc.noaa.gov/data-access/weather-balloon/integrated-global-radiosonde-archive). IGRA contains quality-assured observations from 1500 globally distributed stations with different periods of record from 1960s to present. For the period of this validation, source of the data is the NCDC real-time Global Telecommunication System (GTS) dataset. Quality assurance procedures are described in detail in Durre et al. (2006). As of 2003, 74 % (35 %) of all soundings reached 100 hPa (10 hPa) level. Average sounding has 46 levels (vertical resolution about 0.5 km).

COSMIC/SuomiNet is a ground-based GPS network designed for real-time remote sensing of atmospheric water vapour. The network provides integrated atmospheric water vapour columns and total electron content from globally distributed GPS stations. Precipitable water estimates are provided for each station at 30 min time resolution (Ware et al., 2000). GPS data were missing for the period from 8 August 2009 to 7 February 2010.

In comparisons between radiosonde and GPS total water vapour observations, radiosondes generally have a wet bias. Igondova (2009) observed wet mean bias of 0.135 kg m^{-2} and the SD of 1.280 kg m^{-2}. Wang and Zhang (2007) observed generally wet biases of 0–4 kg m^{-2}. Bias, however, varies considerably, depending on water vapour amount, time of day and instruments used.

4 Data selection and co-locations

In all comparisons, the GOME-2 measurements were screened for cloudy scenes. Two separate cloud indicators are used to flag the cloudy pixels. The first cloud flag is set if the effective cloud fraction (product of cloud top albedo and geometric cloud fraction) exceeds 0.6, indicating a very high cloud top reflection. The second cloud flag is set when the retrieved O_2 slant column is below 80 % of the maximum for the respective solar zenith angle. This requirement ensures that the main part of the O_2 slant column used in the calculation of air mass factor correction is visible. Both flags were used in the screening.

The measurements with solar zenith angle greater than 75° were discarded in order to exclude low light conditions. Only forward-scan pixels were used for comparisons, since back-scan pixels are of a larger size and are currently not recommended for use. Of the forward-scan co-locations available, about 20 % have solar zenith angle greater than 75°, 20 % have the first cloud flag set and 50 % have the second cloud flag set. This leaves about 40 % of the co-locations for comparisons. GOME-2A observations are compared from January 2007 to July 2013 and GOME-2B observations from the 13 December 2012 to July 2013. Data used in the comparisons are processed using the GDP version 4.7, operational since July 2013.

For our analysis, we selected GOME-2 measurements that are co-located with the radio soundings within GOME-2 pixel and within three hours of Metop overpass. This means that the centres of GOME-2 pixels (nominally 40 km × 80 km) are within 50 km of sonde launch sites in majority of cases. Water vapour columns were calculated

by integrating from surface up to the altitude of the lapse-rate tropopause, which is specified in the IGRA profiles. Soundings without specified tropopause were discarded. Only profiles with more than 20 altitude levels were used for the analysis. Screening for incomplete soundings removes about 18 % of the co-locations. After screening, total number of co-locations with radiosonde was about 480 000 for GOME-2A and 44 000 for GOME-2B.

Similarly, GOME-2 and GPS measurements co-located within GOME-2 pixels were used, but because of better temporal resolution of GPS measurements, observations with smallest available time difference were selected for each co-location. If the GPS measurements are available for full day, time difference between GOME-2 overpass and GPS measurement is less than 15 min. We have used only GPS measurements that have the formal (as specified in data files) error term not exceeding 0.3. Screening for formal error removes 0.3 % and the requirement for 15 min maximum time difference 3 % of the co-locations. Total number of co-locations with GPS was about 94 000 for GOME-2A and 9000 for GOME-2B. Locations of the co-located observations for both radiosondes and GPS observations are shown in Fig. 1.

5 Results and discussion

5.1 Overall agreement

In order to illustrate the overall agreement between the datasets, we present the scatter plots of GOME-2A and GOME-2B measurements vs. co-located radiosonde and GPS measurements. For each range of ground-based water vapour column values, we computed the percentiles of GOME-2 distributions. In Fig. 2, we indicated the median (solid thick line), 5th and 95th percentiles (thin solid lines), and 25th and 75th percentiles (dashed lines). As observed in Fig. 2, moderate values of GOME-2 water vapour are in a very good agreement with both radiosonde and GPS data, while large water vapour abundances are smaller in GOME-2 datasets than in the collocated

ground-based data. This suggests that GOME-2 water vapor estimates are less reliable above 50 kg m^{-2}. The range and number of outliers (i.e., large differences, which are seen in Fig. 2), is however smaller in comparison with GPS than in the comparison with sondes. This might be due to a smaller time difference between GOME-2 and GPS measurements, or due to a more robust water vapour estimates in GPS data.

The statistics of the overall comparison are shown in Table 1. Good correlation of both GOME-2A and GOME-2B with ground-based data is observed, with the correlation coefficient of 0.91 against radiosondes and 0.94 against GPS. GOME-2 data show negative (dry) median difference against radiosondes and positive (wet) median difference against GPS observations. This agrees also with the differences between radiosonde and GPS data reported in Wang and Zhang (2007). The mean relative differences are fairly large due to very high relative differences seen at low values (see also below).

The shape of the scatter plots (Fig. 2) suggests that the overall biases depend on water vapour abundances. This is clearly observed in Fig. 3, which shows median relative differences and 5th, 25th, 75th and 95th percentiles as a function of ground-based observations. For water vapour values in the range of 8–50 kg m^{-2}, the relative differences between GOME-2 and ground-based observations are small, within ±5 %. At low H_2O values, below 8 kg m^{-2}, a large positive bias of GOME-2 is clearly visible, especially in comparisons against the GPS data.

Figure 4 shows the time series of the global monthly median difference (GOME-2 – ground) with 5th, 25th, 75th and 95th percentiles of the monthly distributions. The global median difference shows some seasonal variations with the magnitude of about 1 kg m^{-2}. No visible drift in the mean differences during the comparison period is observed. The estimated drifts are very small, less than 0.005 kg m^{-2} dec^{-1} (less than 0.03 % dec^{-1}), and they are not statistically significant. No significant difference can be seen in behaviour of GOME-2A and B.

5.2 Classification of the biases

The validation studies of the previous GOME-2 processor versions have shown the strong dependence of GOME-2 water vapour on the scan angle (e.g., Noël et al., 2008). In the GDP v.4.7, the scan angle dependency of the measurements has been removed to large extent by the semi-empirical corrections (details can be found in Grossi et al., 2014). To investigate the quality of the applied scan-angle correction, we show the median relative difference of GOME-2A and B observations against radiosonde and GPS observations for different line-of-sight zenith angles, as well as 5th, 25th, 75th and 95th percentiles of the distribution (Fig. 5).

Negative zenith angles in Fig. 5 refer to the eastern half of the swath and positive ones to the western. As observed in Fig. 5, the scan-angle dependence of GOME-2 H_2O data is small. However, the western edge of the GOME-2 swath shows about 5 % higher water vapour column than the eastern one in comparisons with the radiosonde observations. In comparisons with the GPS observations, both edges of the swath show wet bias about 10 % compared to the center of the swath.

As discussed in Grossi et al. (2014) the quality of GOME-2 water vapour data might depend on solar zenith angle, surface albedo and the cloud fraction due to approximations in the retrieval algorithm. To investigate the influence of this factors, the relative differences between GOME-2A and GOME-2B data and the collocated radiosonde observations are presented as functions of solar zenith angle, geometric cloud fraction and surface albedo (Fig. 6). The median deviations from radiosonde data depend weakly on solar zenith angle, they are 5–10 % higher for larger solar zenith angles. Scatter of the relative difference distribution can be seen to increase with increasing solar zenith angle. This is probably due to a larger fraction of data with smaller water vapour abundances observed at large solar zenith angles.

In our analysis, we have applied the cloud screening. Despite this, the difference of similar magnitude can be seen for observations with very small or large geometric cloud

fraction, compared to observations in moderately cloudy situations (Fig. 6, center). The range of these variations is about 15 %.

As observed in Fig. 6 (right), surface albedo has the largest impact on the differences with respect to the radiosonde data. The cases corresponding to different surface albedos show significantly different biases: from the positive (wet) bias of up to 10 % for very dark surfaces (albedo < 0.1) to the negative bias up 20 % for observations with albedo above 0.3. Table 2 shows the statistics of the comparisons of GOME-2A observations with radiosondes over different surface types (land, sea or snow/ice). Biases seen here agree with the ones observed in Fig. 6 (right). Sea pixels (very low albedos) show positive bias, while pixels classified as ice or snow (high albedos) show large negative biases. In GOME-2 retrievals, the surface albedo map is the only external information (Grossi et al., 2014); it has rather large uncertainties, especially over oceans where the information about albedo is limited. Future developments of the GOME-2 algorithm and the surface albedo databases might resolve this problem.

The illustration of the seasonal and latitudinal dependence of the biases with respect to the ground-based datasets is presented in Fig. 7. Here, we computed monthly zonal medians of relative differences between GOME-2 and ground-based measurements in 10° latitude zones. When compared with sondes, GOME-2A generally has a wet bias in the Southern Hemisphere and a dry bias in the Northern Hemisphere. Seasonal variations in the differences can be seen at mid-latitudes, especially in the Southern Hemisphere. These seasonal variations at mid-latitudes are in a broad agreement with the general dependence of GOME-2 biases shown in Fig. 3: a negative/smaller bias in wet seasons (summer) and a positive/larger bias in dry seasons (winter). Comparisons with GPS show a wet bias in most areas with a stronger bias in the Southern Hemisphere. We would like to note that the seasonal-latitudinal structures presented in Fig. 7 are difficult for interpretation because of the following reasons. First, the number on collocated measurements in the latitude-month bins is quite different (see Fig. 8). This means that the bias estimates for some bins may not be statistically significant. Second, as discussed in Grossi et al. (2014), the GOME-2 biases have a pronounced

zonal structure (which is associated with e.g. surface albedo, as discussed also in our paper), while the ground-based stations are distributed highly non-uniformly in longitude, especially GPS stations. Third, some of the large differences observed in comparison against GPS observations are the result of large differences observed at a few stations. Let us consider the latitude zone 20–30° N, for example. As shown in Fig. 7, a large positive bias against GPS is observed starting from May 2011, while such a bias in not observed in comparisons with radiosondes. A large fraction of the data in this latitude zone is from the stations at 27–28° N, 15–17° W (both radiosonde and GPS stations are available). Figure 9 shows an example time series of the collocated GOME-2A and ground observations at radiosonde and GPS stations in this region located less than 100 km from each other. While the radiosonde observations generally match the GOME-2A very closely, GPS observations are much lower. This explains the strange appearance of strong bias in comparisons with GPS at 20–30° N after May 2011. Excluding such peculiarities, the overall distributions shown in Fig. 7 are in a broad agreement with the magnitude and the structure of biases discussed in Sect. 5.1.

6 Conclusions

We have performed the global validation of O3M SAF total column water vapour from GOME-2A (January 2007 to August 2013) and GOME-2B (December 2012 to August 2013) using radiosonde data from IGRA archive and the GPS data from COSMIC/SuomiNet network. Overall, GOME-2 data have shown a good agreement with both correlative datasets. Correlation coefficients are higher than 0.9 for all comparisons. Small dry negative median differences (GOME-2A: −2.7 %, GOME-2B: −0.3 %) are observed against the radiosondes, while against the GPS wet median difference (GOME-2A: 4.9 %, GOME-2B: 3.2 %) is observed. Moderate values of GOME-2 water vapour of 8–50 $kg\,m^{-2}$ are in a very good agreement with both radiosonde and GPS data (the relative difference is within ±5 %), while high H_2O values show a pronounced

dry bias and small H_2O values exhibit a strong wet bias, in all comparisons. A strong dependence on GOME-2 biases on surface albedo is found, from the positive (wet) bias of up to 10 % for very dark surfaces (albedo < 0.1) to the negative bias up 20 % for observations with albedo above 0.3. The dependence of GOME-2 biases on solar zenith angle and cloudiness is smaller; the relative differences with respect to radiosonde data vary within 15 %. GOME-2A generally shows good ability to represent the seasonal variations of water vapour. No trend in median difference with the radiosonde data is apparent during the validation period. Notably the behaviour of GOME-2A and B was very similar in all comparisons. This opens the opportunity for combined use of the GOME-2A and GOME-2B data.

Acknowledgements. Authors thank Integrated Global Radiosonde Archive (IGRA) for radiosonde data and COSMIC/Suominet project for GPS data.

Validation of GOME-2 Total Water Vapour was funded by EUMETSAT Satellite Application Facility on Ozone and Atmospheric Chemistry Monitoring (O3M SAF) and Finnish Academy projects CLASP and ASTREX.

References

Anthes, R. A., Ector, D., Hunt, D. C., Kuo, Y-H., Rocken, C., Schreiner, W. S., Sokolovskiy, S. V., Syndergaard, S., Wee, T-K., Zeng, Z., Bernhardt, P. A., Dymond, K. F., Chen, Y., Liu, H., Manning, K., Randel, W. J., Trenberth, K. E., Cucurull, L., Healy, S. B., Ho, S.-P., McCormick, C., Meehan, T. K., Thompson, D. C., and Yen, N. L.: The COSMIC/FORMOSAT-3 Mission: Early Results. Bull. Amer. Meteor. Soc., 89, 313–333, 2008. 12519

Bennartz, R. and Fischer, J.: Retrieval of columnar water vapour over land from backscattered solar radiation using the Medium Resolution Imaging Spectrometer, Remote Sens. Environ., 78, 274–283, 2001. 12519

Chaboureau, J.-P., Chédin, A., and Scott, N. A.: Remote sensing of the vertical distribution of atmospheric water vapor from the TOVS observations: method and validation, J. Geophys. Res.-Atmos., 103, 8743–8752, 1998. 12519

du Piesanie, A., Piters, A. J. M., Aben, I., Schrijver, H., Wang, P., and Noël, S.: Validation of two independent retrievals of SCIAMACHY water vapour columns using radiosonde data, Atmos. Meas. Tech., 6, 2925–2940, doi:10.5194/amt-6-2925-2013, 2013. 12521

Durre, I., Vose, R. S., and Wuertz, D. B.: Overview of the integrated global radiosonde archive, J. Climate, 19, 53–68, 2006. 12522

Gao, B. C. and Kaufman, Y. J.: Water vapor retrievals using Moderate Resolution Imaging Spectroradiometer (MODIS) near-infrared channels, J. Geophys. Res.-Atmos., 108, 4389, doi:10.1029/2002JD003023, 2003. 12519

Grossi, M., Valks, P., Loyola, D., Aberle, B., Slijkhuis, S., Wagner, T., Beirle, S., and Lang, R.: Total column water vapour measurements from GOME-2 MetOp-A and MetOp-B, Atmos. Meas. Tech. Discuss., 7, 3021–3073, doi:10.5194/amtd-7-3021-2014, 2014. 12520, 12522, 12526, 12527

Igondova, M.: Analysis of precision and accuracy of precipitable water vapour derived from GPS observations, Contributions to Geophysics and Geodesy, 39/2, 121–132, 2009. 12523

Kiehl, J. T. and Trenberth, K. E.: Earth's annual global mean energy budget, B. Am. Meteorol. Soc., 78, 197–208, 1997. 12518

King, M. D., Kaufman, Y. J., Menzel, W., and Tanre, D.: Remote sensing of cloud, aerosol, and water vapor properties from the Moderate Resolution Imaging Spectrometer (MODIS), IEEE T. Geosci. Remote, 30, 2–27, 1992. 12519

Li, J., Wolf, W. W., Menzel, W. P., Zhang, W., Huang, H. L., and Achtor, T. H.: Global soundings of the atmosphere from ATOVS measurements: the algorithm and validation, J. Appl. Meteorol., 39, 1248–1268, 2000. 12519

Mieruch, S., Schröder, M., Noël, S., and Schulz, J.: Comparison of monthly means of global total column water vapor retrieved from independent satellite observations, J. Geophys. Res.-Atmos., 115, D23310, doi:10.1029/2010JD013946, 2010. 12521

Noël, S., Buchwitz, M., Bovensmann, H., Hoogen, R., and Burrows, J. P.: Atmospheric water vapor amounts retrieved from GOME satellite data, Geophys. Res. Lett., 26, 1841–1844, 1999. 12519, 12521

Noël, S., Buchwitz, M., Bovensmann, H., and Burrows, J. P.: Retrieval of total water vapour column amounts from GOME/ERS-2 data, Adv. Space Res., 29, 1697–1702, 2002. 12519

Noël, S., Buchwitz, M., and Burrows, J. P.: First retrieval of global water vapour column amounts from SCIAMACHY measurements, Atmos. Chem. Phys., 4, no. 1, 111–125, 2004. 12519

Noël, S., Buchwitz, M., Bovensmann, H., and Burrows, J. P.: Validation of SCIAMACHY AMC-DOAS water vapour columns, Atmos. Chem. Phys., 5, 1835–1841, doi:10.5194/acp-5-1835-2005, 2005. 12521

Noël, S., Mieruch, S., Bovensmann, H., and Burrows, J. P.: Preliminary results of GOME-2 water vapour retrievals and first applications in polar regions, Atmos. Chem. Phys., 8, 1519–1529, doi:10.5194/acp-8-1519-2008, 2008. 12520, 12526

Schlüssel, P. and Emery, W. J.: Atmospheric water vapour over oceans from SSM/I measurements, Int. J. Remote Sens., 11, 753–766, 1990. 12519

Susskind, J., Barnet, C. D., and Blaisdell, J. M.: Retrieval of atmospheric and surface parameters from AIRS/AMSU/HSB data in the presence of clouds, IEEE T. Geosci. Remote, 41, 390–409, 2003. 12519

Valks, P., Loyola, D., Hao, N., Hedelt, P., Slijkhuis, S., and Grossi, M.: Algorithm Theoretical Basis Document for GOME-2 Total Column Products of Ozone, Tropospheric Ozone, NO_2, Tropospheric NO_2, BrO, SO_2, H_2O, HCHO, OClO and Cloud Properties, 21 May 2013a. 12522

Valks, P., Loyola, D., Zimmer, W., Kiemle, S., Hao, N., Hedelt, P., Grossi, M., Pedergnana, M., Emmadi, S., Butenko, L., and Livschitz, Y.: Product User Manual for GOME Total Columns of Ozone, NO_2, tropospheric NO_2, BrO, SO_2, H_2O, HCHO, OClO, and Cloud Properties, 21 May 2013b. 12522

Wagner, T., Heland, J., Zöger, M., and Platt, U.: A fast H_2O total column density product from GOME – Validation with in-situ aircraft measurements, Atmos. Chem. Phys., 3, 651–663, doi:10.5194/acp-3-651-2003, 2003. 12521

Wagner, T., Beirle, S., Grzegorski, M., Sanghavi, S., and Platt, U.: El Niño induced anomalies in global data sets of total column precipitable water and cloud cover derived from GOME on ERS-2, J. Geophys. Res.-Atmos., 110, , D15104, doi:10.1029/2005JD005972, 2005. 12521

Wagner, T., Beirle, S., Grzegorski, M., and Platt, U.: Global trends (1996–2003) of total column precipitable water observed by Global Ozone Monitoring Experiment (GOME) on ERS-2 and their relation to near-surface temperature, J. Geophys. Res.-Atmos., 111, D12102, doi:10.1029/2005JD006523, 2006. 12521

Wang, J. and Zhang, L.: Systematic errors in global radiosonde precipitable water data from comparisons with ground-based GPS measurements, J. Climate, 21, 2218–2238, 2008. 12523, 12525

Ware, R. H., Fulker, D. W., Stein, S. A., Anderson, D. N., Avery, S. K., Clark, R. D., Droegemeier, K. K., Kuettner, J. P., Minster, J. B., and Sorooshian, S.: Suominet: a real-time national GPS network for Atmospheric Research and education, B. Am. Meteorol. Soc., 81, 677–694, 2000. 12522

Table 1. Statistics of comparisons between GOME-2A and B with radiosondes and GPS observations.

	correlation coefficient	mean difference	mean relative difference	standard deviation	median difference	median relative difference
GOME-2A – Sonde	0.910	$-0.44\,kg\,m^{-2}$	0.38 %	$5.27\,kg\,m^{-2}$	$-0.32\,kg\,m^{-2}$	−2.7 %
GOME-2A – GPS	0.936	$0.63\,kg\,m^{-2}$	14.9 %	$4.48\,kg\,m^{-2}$	$0.50\,kg\,m^{-2}$	4.9 %
GOME-2B – Sonde	0.909	$0.03\,kg\,m^{-2}$	11.8 %	$5.53\,kg\,m^{-2}$	$-0.03\,kg\,m^{-2}$	−0.3 %
GOME-2B – GPS	0.941	$0.25\,kg\,m^{-2}$	16.8 %	$4.51\,kg\,m^{-2}$	$0.33\,kg\,m^{-2}$	3.2 %

Table 2. Statistics of comparisons between GOME-2A with radiosondes over different surface types

	correlation coefficient	mean difference	mean relative difference	standard deviation	median difference	median relative difference
Land	0.901	$-0.98\,kg\,m^{-2}$	−2.3 %	$5.10\,kg\,m^{-2}$	$-0.60\,kg\,m^{-2}$	−4.3 %
Sea	0.906	$1.45\,kg\,m^{-2}$	12.0 %	$6.15\,kg\,m^{-2}$	$1.37\,kg\,m^{-2}$	9.2 %
Ice	0.855	$-1.21\,kg\,m^{-2}$	−15.0 %	$2.28\,kg\,m^{-2}$	$-0.93\,kg\,m^{-2}$	−19.2 %

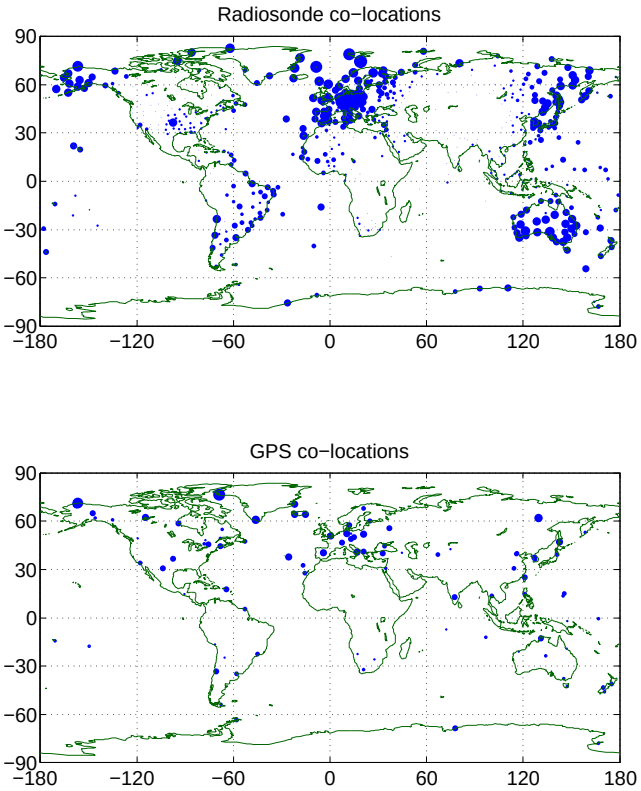

Figure 1. Locations of the GOME-2A co-locations with radiosondes (top) and GPS (bottom). Size of the markers is proportional to the number of co-located data.

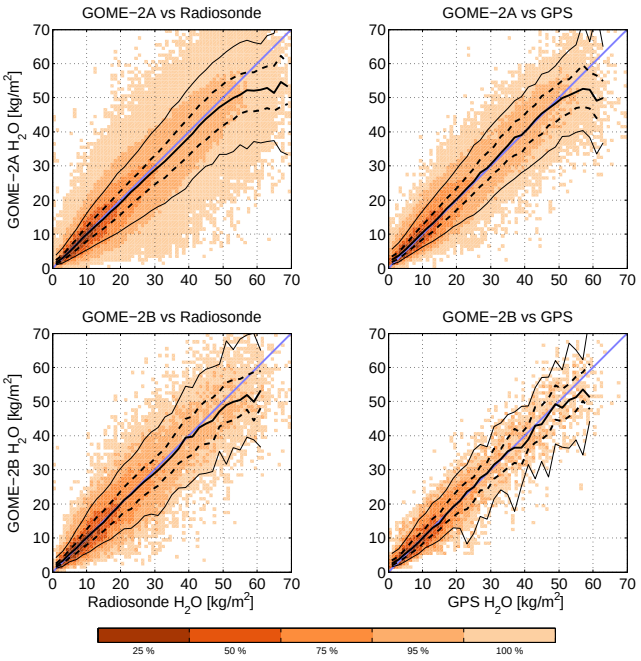

Figure 2. Scatter plot of GOME-2A (top) and GOME-2B (bottom) total water vapor columns against the IGRA integrated total water vapor columns (left) and COSMIC/SuomiNet GPS water vapor (right). Color represents the fraction of hits, solid line is the median of the GOME-2 water vapour column in 2 kg m^{-2} bin, dashed lines 25 and 75 % percentiles and thin solid lines 5 and 95 % percentiles. Solid blue line is $x = y$ line.

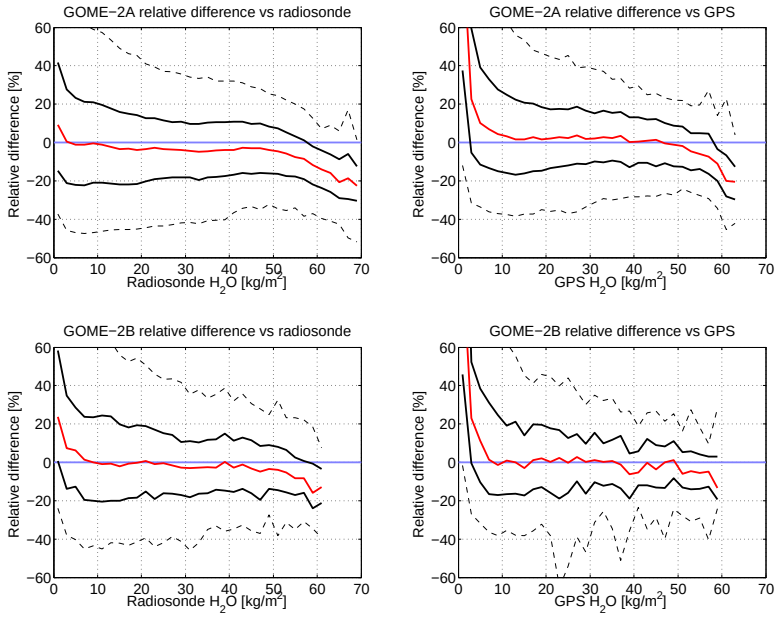

Figure 3. Median relative differences (red solid line), 25 and 75 % percentiles (black solid lines) and 5 and 95 % percentiles (dashed lines) for GOME-2A (top) and GOME-2B (bottom) against radiosonde (left) and GPS (right).

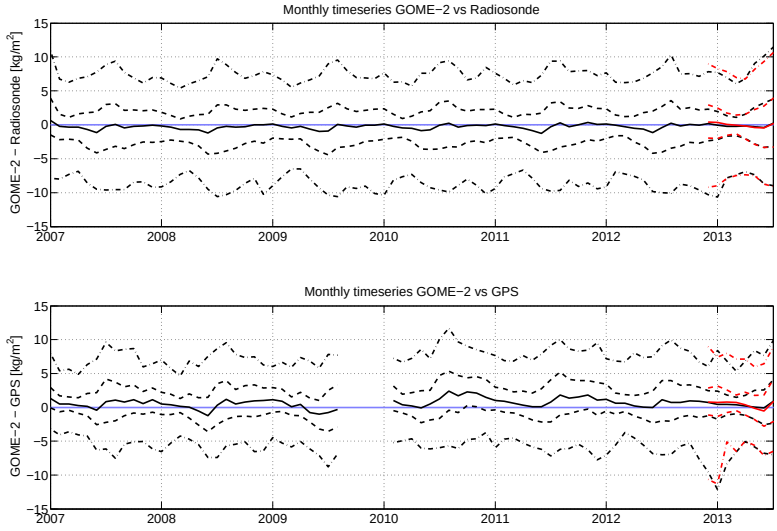

Figure 4. Time series of global monthly median differences (solid line), 25 and 75 % percentiles (dashed lines) and 5 and 95 % percentiles (dash-dot lines) for GOME-2A (black) and GOME-2B (red) against radiosonde (top) and GPS (bottom).

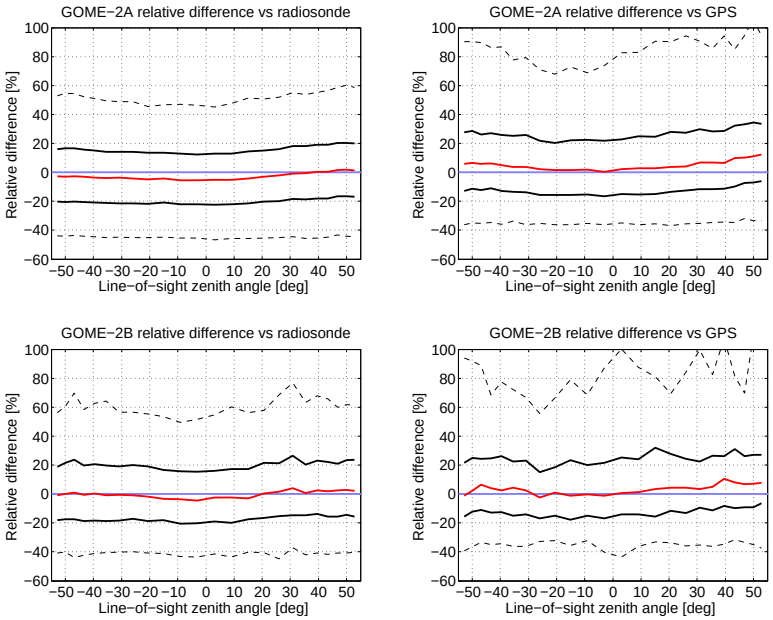

Figure 5. Median relative differences (red solid line), 25 and 75 % percentiles (black solid lines) and 5 and 95 % percentiles (dashed lines) for GOME-2A (top) and GOME-2B (bottom) against radiosonde (left) and GPS (right) as a function of line-of-sight zenith angle at the centre of the GOME-2 pixel. Negative angles correspond to the eastern edge of the swath and positive to the western. Only observations from full-swath (1920 km) scans are used in analysis.

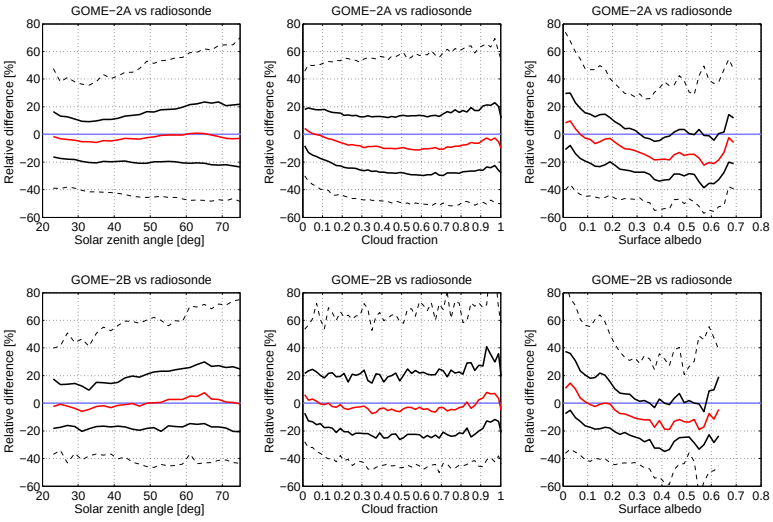

Figure 6. Median relative differences (red solid line), 25 and 75 % percentiles (black solid lines) and 5 and 95 % percentiles (dashed lines) for GOME-2A (top) and GOME-2B (bottom) against radiosonde as a function of solar zenith angle (left), geometric cloud fraction (center) and surface albedo (right).

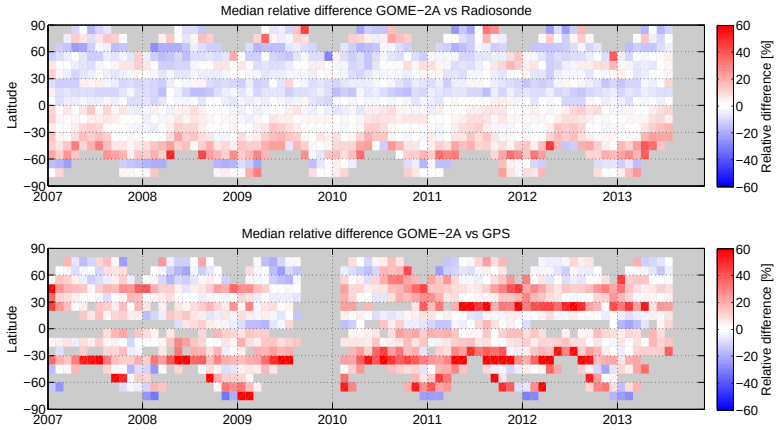

Figure 7. Monthly median relative difference [%] as a function of time and latitude, GOME-2A vs. radiosonde (top) and GPS (bottom). Each coloured box shows the median relative difference for one month in 10° latitude zone. Month-latitude bins with less than 10 co-locations are not shown.

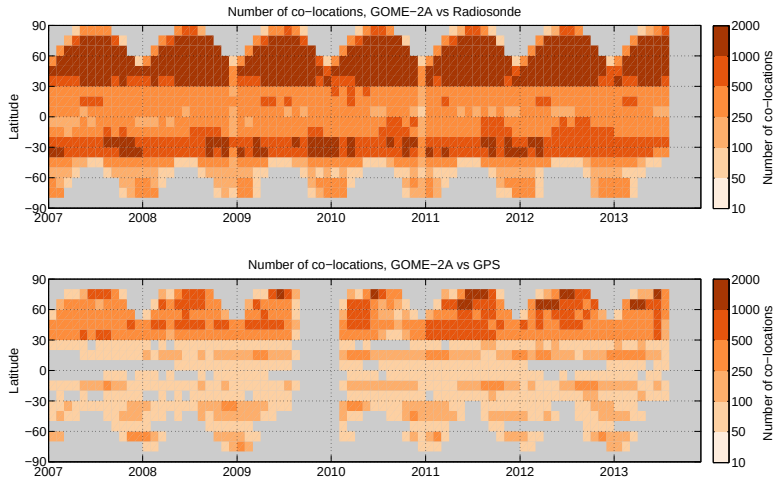

Figure 8. Number of co-locations per month and 10° latitude zone, for GOME-2A vs. radiosonde (top) and GPS (bottom).

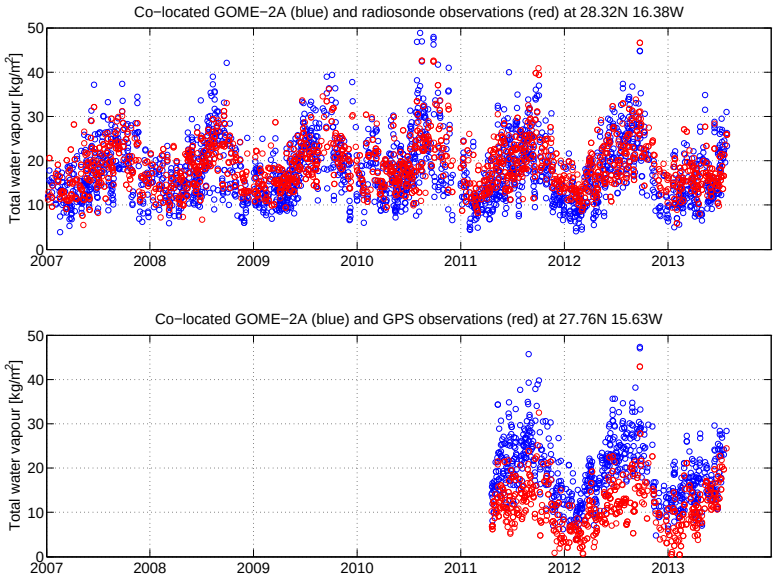

Figure 9. Top: time-series of co-located observations for GOME-2A (blue) and radiosonde (red) at 28.32° N, 16.38° W. Bottom: GOME-2A (blue) and GPS (red) at 27.76° N, 15.63° W.